Chapter 4

Synthesis and Characterization of Glass Fiber Reinforced BMI-Epoxy-$BaTiO_3$ Nanocomposites

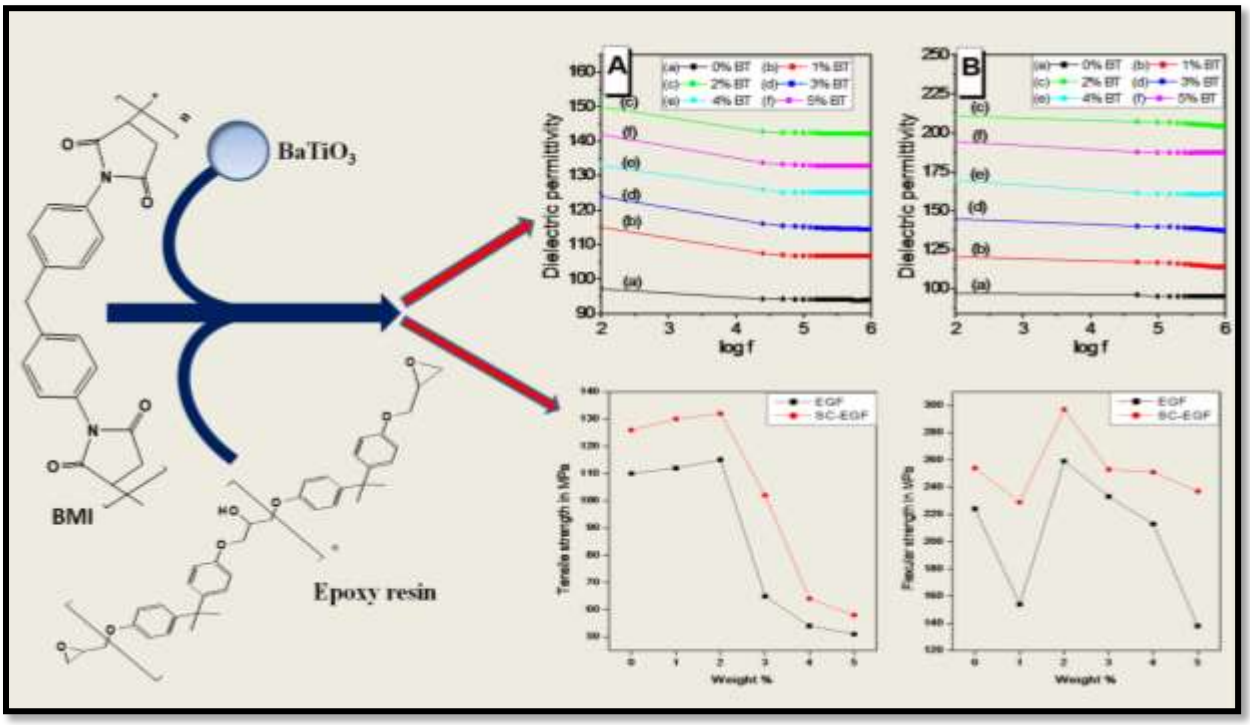

Chapter 4

Synthesis and characterisation of glass fiber reinforced BMI-Epoxy-$BaTiO_3$ Nanocomposites

Abstract

Bismaleimide-epoxy-$BaTiO_3$ (BMI-epoxy-BT) glass fiber reinforced composites were prepared using E-glass fiber (EGF) and silane coated E-glass fiber (SC-EGF) separately as reinforcement. $BaTiO_3$ nanoparticles were prepared by hydrothermal method. Results show that the addition of $BaTiO_3$ nanoparticles has significant effects on the mechanical and dielectric properties of the composite. EGF and SC-EGF reinforced BMI-epoxy-BT composites with 2 weight % of $BaTiO_3$ nanoparticles showed improved tensile strength, flexural strength and dielectric constant and those with 3 weight % showed high dielectric strength indicating this composition is more adaptable for high dielectric applications. Dielectric constants and dielectric loss of the fabricated nanocomposites have been obtained at higher frequencies (in GHz) by using vector network analyser at room temperature and was found to be highest for the BMI-epoxy nanocomposite with 1 weight % nanofiller.

4.1. Introduction

Bismaleimide (BMI) is a high performance thermosetting polyimide and find applications in radar, space ware composites, stealth areas, supercapacitors, PCB [1,2] etc. Unmodified BMI composites owing to high crosslinking density during curing are brittle in nature [3,4]. In order to overcome its brittleness, structural modifications, co-reactions, blending with suitable compounds, glass fiber or carbon fiber reinforcement are adopted. Epoxy resins are widely used as matrix materials for high performance composites. In order to enhance both the temperature performance and the processing ease, BMI is blended with epoxy resins[5–10]. High dielectric permittivity is a prerequisite for the dielectric materials used in embedded capacitors and energy storage devices[11–13]. In order to enhance the dielectric properties of BMI composites suitable nanofillers with a high dielectric constant are added.

Barium titanate (BT) is a dielectric ceramic material with multidimensional properties such as piezoelectric, ferroelectric[14–19], pyroelectric and photorefractive properties. $BaTiO_3$ also has electro optic modulating properties at high GHz frequencies, NTCR

properties in single crystals[20], PTCR properties in polycrystalline forms[21,22] and phase transition at different temperatures. This envisages the widespread use of BT in electrical insulators[23], energy storage systems[24,25], capacitors[26], MLCCs[27], sensors[28,29], thermistors[30,31], electro optical devices [32,33] etc.

Dielectric properties of BT ceramics depend on grain size and applied frequency[35, 36]. Dielectric constant increases with decrease in grain size. BT with grain size 10 micron exhibits dielectric constant in the range 1500-2000 and those with grain size approximately 1 micron are capable of exhibiting dielectric constant in the range 3500-6000 at room temperature. Values as high as 15000 are possible for BT in nanosize[34]. BT nanoparticles were synthesised by hydrothermal method. The major advantage of this method is the production of BT powders in the nanosize range of 50-400 nm with spherical structural characteristics and monodispersity compared to that prepared by the solid state reaction methods. XRD also reveals the cubic structure of BT powders synthesised by hydrothermal method at low temperatures.

To improve the mechanical properties of nanocomposite, E glass fiber (EGF) and silane coated E glass fiber (SC-EGF) are reinforced separately into bismaleimide resin matrix via hand layup method and tested for dielectric properties and mechanical properties like tensile strength and flexural strength[35].

This work is focused on the effect of BT nanoparticles on the dielectric, mechanical and thermal properties of bismaleimide – epoxy composites reinforced with glass fiber. BT nanoparticles synthesised by hydrothermal method were characterised using scanning electron microscopy (SEM), powder X-ray diffraction (XRD) and FTIR. The synthesised $BaTiO_3$ nanoparticles were incorporated into bismaleimide–epoxy matrix in varying percentages and the parameters were investigated.

4.2. Experimental

4.2.1. Preparation of $BaTiO_3$ (BT) nanoparticles

BT nanoparticles were synthesised by hydrothermal method from $Ti(C_4H_9O)_4$ and $Ba(OH)_2.8H_2O$ precursors[36–42]. Typically, 1ml of $Ti(C_4H_9O)_4$ was added to 18 ml ethanol solution in drops with continuous stirring followed by the slow addition of 0.06 ml HNO_3 and 3 ml distilled water. 10 ml of this freshly prepared solution was added dropwise into an aqueous Ba $(OH)_2$ solution whose concentration was 1.0 M, with continuous stirring. This mixture was transferred into a teflon lined autoclave

maintained at 200°C and kept for 16 hours. The autoclave was cooled to room temperature, products were filtered, washed with distilled water-ethanol mixture and dried at 60°C under vacuum for 24 hours[43].

4.3. Results and discussion

4.3.1. Thermogravimetric analysis

TGA curves of cured BMI, BMI-epoxy and BMI-epoxy composite with 2 weight % of BT nanofiller without glass fiber were illustrated in figure 4.1. From the TGA curves it is clear that BMI-epoxy composite with 2 weight % BT has higher thermal stability than BMI resin and BMI-epoxy composite which may be due to the interaction of the dispersed BT nanofiller with adjacent polymer matrix layers. The addition of filler not only improve the thermal stability of nanocomposites facilitated by their low migration characteristics but also ensures better compatibility[44]. Weight loss percentages of BMI resin, BMI-epoxy composite 2 weight % BT and BMI-epoxy composite are recorded in table 4.1.

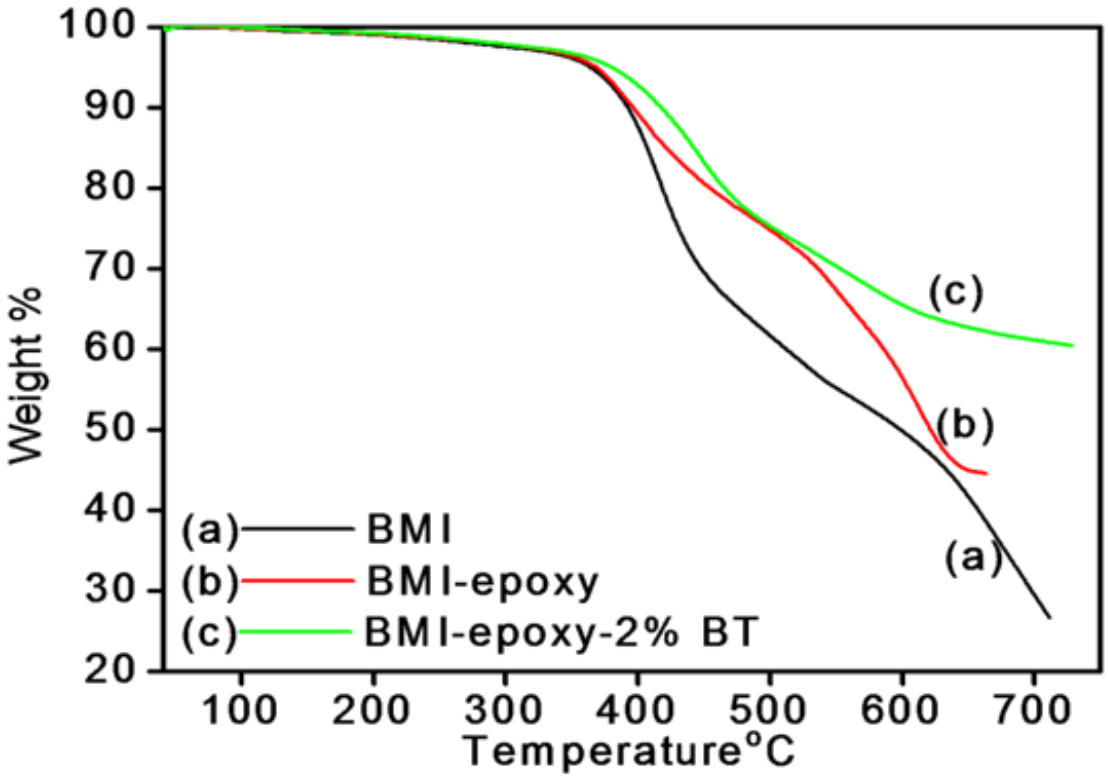

Figure 4.1 TGA curves of (a) BMI resin (b) BMI-epoxy nanocomposite without filler (c) BMI-epoxy composite with 2 weight % BT nanofiller.

Table .4.1 Weight loss percentages of samples obtained from TGA curves.

Sample	Total weight % at 661°C	T 5% (Initial thermal decomposition temperature)
BMI resin	39	362°C
BMI-epoxy composite without filler	45	368°C
BMI-epoxy composite with 2 weight % of BT nanofiller	62.20	380°C

4.3.2. Morphology of BMI-epoxy nanocomposites

SEM images (figure 4.2 A) indicated the existence of BT as spherically shaped nanoparticles. Figure 4.2 B is the elemental dispersive X-ray (EDAX) spectrum of the synthesised BT nanoparticles which confirms the formation of $BaTiO_3$ having a composition of barium 55.05%, titanium 22.45% and oxygen 22.5%, recorded in Table 4.2.

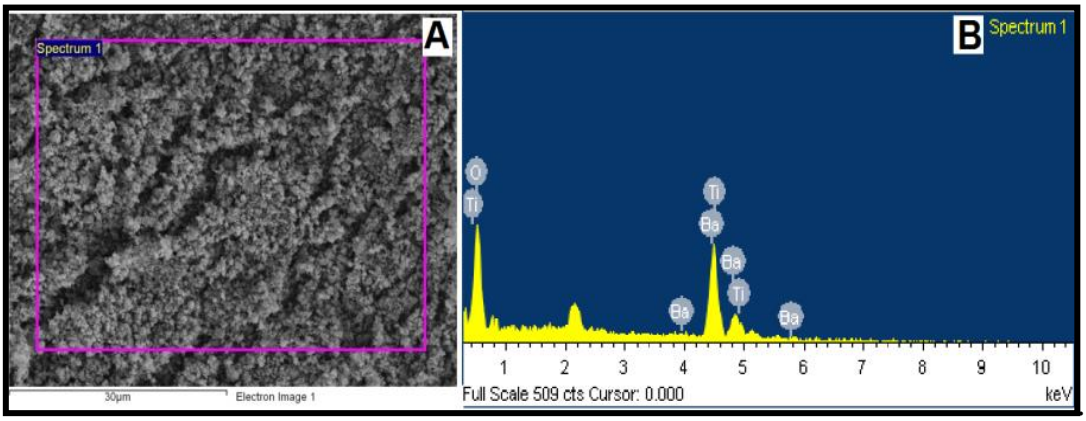

Figure 4.2 SEM image (A) and EDAX (B) of $BaTiO_3$ nanoparticles.

Table 4.2 Weight and atomic percentages of various elements present in $BaTiO_3$ nanoparticles obtained from EDAX.

Element	Weight %	Atomic %
O	17.46	55.05
Ti	21.31	22.45
Ba	61.23	22.50
Total	100	100

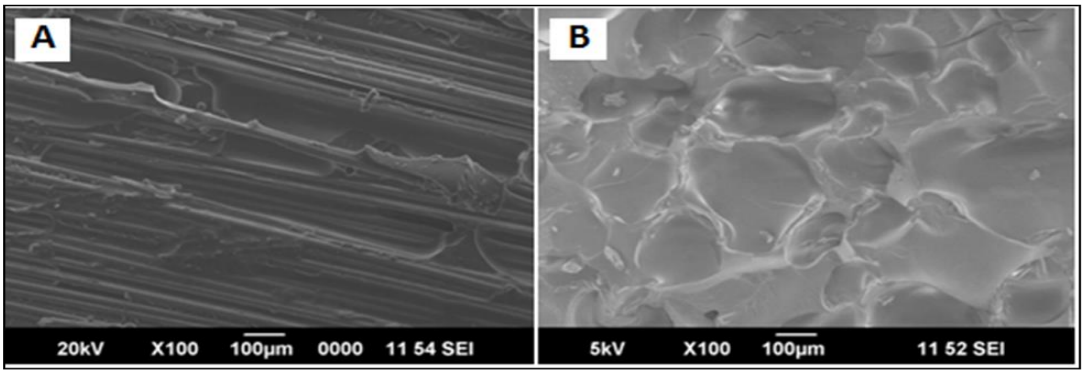

Figure 4.3 SEM images of A) BMI-epoxy composite B) BMI resin.

The morphological variation of BMI resin as well as BMI-epoxy matrix is depicted in figure 4.3. The defective void like surface of BMI resin changes to a more dense like structure in BMI-epoxy matrix indicating good compatibility between the blended polymers which was also complemented by FTIR studies confirming the inter crosslinking between BMI and epoxy. (Refer section 4.3.4 figure 4.12).

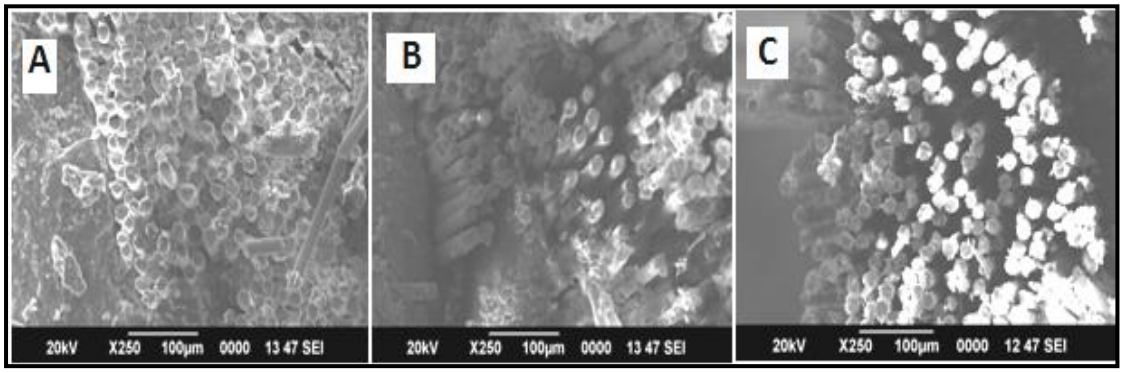

Figure 4.4 Cross sectional SEM images of BMI-epoxy nanocomposites with (A) 1 weight *% (B) 2* weight *% (C) 3* weight *% of BT nanoparticles.*

Figure 4.4 shows the cross sectional SEM images of BMI-epoxy nanocomposites with BT nanoparticles. The glass fibers are sandwiched between the layers of composites and the latter are seen as spherical rods.

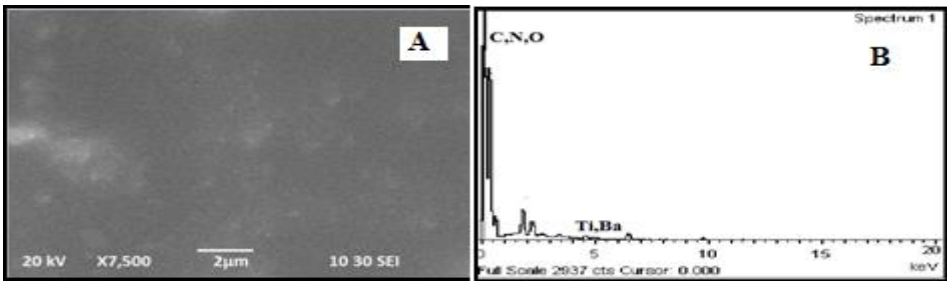

Figure 4.5 (A) SEM and (B) EDAX of BMI-epoxy nanocomposite containing 2 weight *% BT.*

From the SEM images of BMI-epoxy BT composites (figure 4.5 A), BT nanoparticles are found to be homogeneously dispersed throughout the polymer matrix without much agglomeration or voids. As a result of this increased dispersion of nanofiller in the polymer matrix, desired dielectric and thermal properties can be achieved. Moreover, the epoxy moiety can induce interaction with BMI resin via ring opening reaction that adds to the enhanced properties.

The highest tensile strength, observed in composite with 2 weight % of the BT nanoparticles may be due to the uniform distribution of nanofiller in the bismaleimide-epoxy matrix and less agglomeration of the nanofiller that facilitated the good interaction between the polymer matrix and nanofiller as evident from SEM images (figure 4.5).

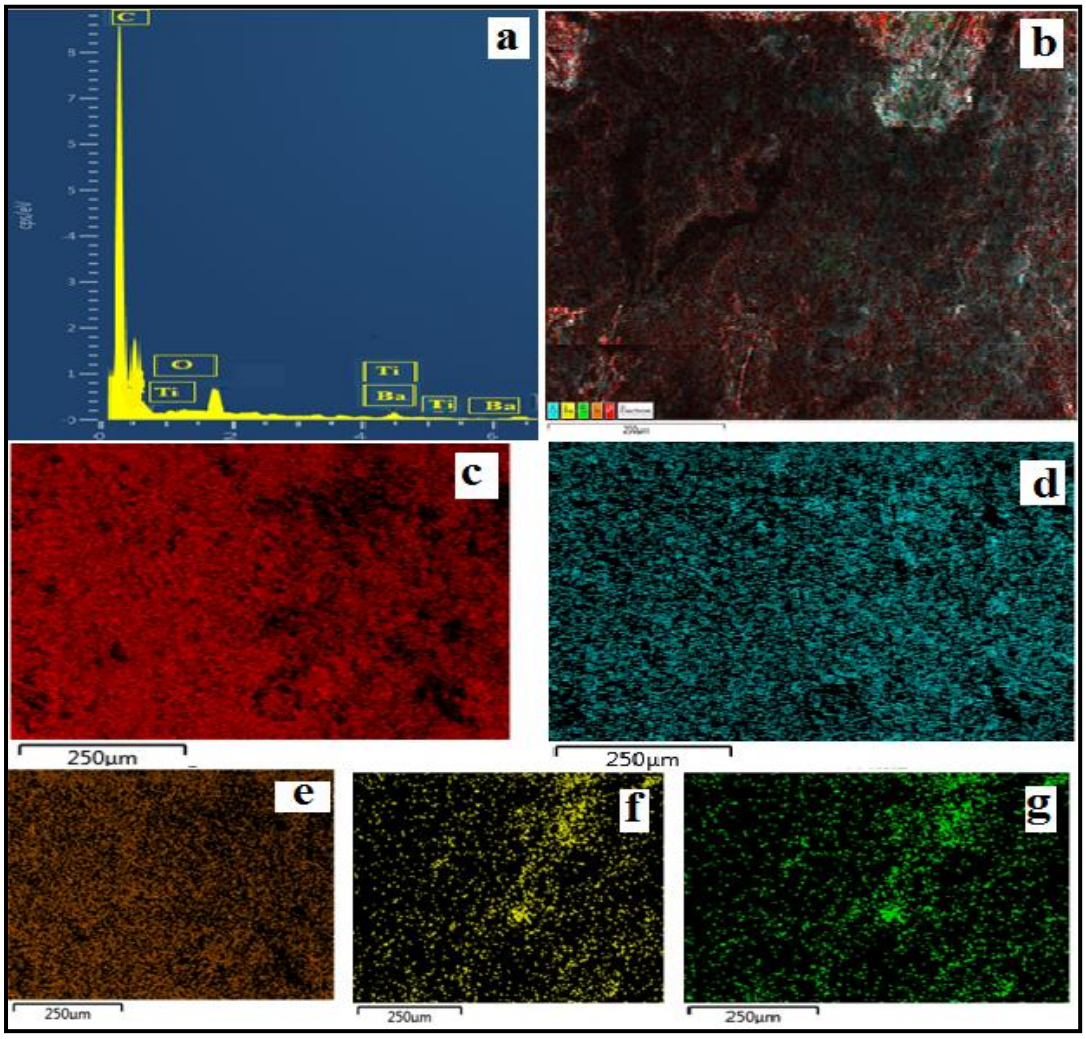

Figure 4.6 (a) EDAX spectra and (b) EDAX mapping of bismaleimide-epoxy composite with 3 weight % BT. EDAX mapping of carbon (c), oxygen (d), nitrogen (e), barium (f) and titanium (g).

From EDAX spectra of BMI-epoxy nanocomposite with 3 weight % BT, overlapped peaks indicates the presence of C (0.277 keV), N (0.392 keV), O (0.525 keV) and Ti (0.39, 0.452, 0.5 & 4.51, 4.5, 4.9 keV). Two less intense peaks between 4.5-5.0 keV indicate the presence of Ti and Ba.

EDAX spectrum of the fabricated BMI-epoxy 3 weight % BT composite (figure 4.6 a) shows the presence of elements carbon, nitrogen and oxygen along with barium and titanium. The absence of any other elements highlights the purity of the fabricated composite. EDAX mapping image (figure 4.6 b) of the composites show the dispersion of all the elements in the composite. EDAX mapping images (figure 4.6 c, d, e, f and g) show the dispersion of individual elements carbon, oxygen, nitrogen, barium and titanium respectively. Proper dispersion of the elements barium and titanium without severe aggregations reveals the proper distribution of BT in the BMI-epoxy matrix.

4.3.3. X-ray diffraction analysis

4.3.3.1. X-ray diffraction analysis of $BaTiO_3$ nanoparticles

XRD pattern of BT matched with JCPDS No #892475. The most intense peak (110) is found at $2\theta = 31.57°$. The peaks at $2\theta = 22.19°$ (100), 31.57° (110), 38.92° (111), 45.27° (200), 50.96° (210), 56.18° (211), 65.87° (220), 70.39° (300), 74.82° (310) and 79.17° (311) confirm perovskite structure of the synthesized BT nanoparticles. Using Scherrer's formula, the average crystallite size of the BT nanoparticles was calculated and found to be around 33 nm.

By comparing the figures 4.7 B (a) and (b) with 4.8 B, it is clear that the narrow diffraction peaks between 2θ range 19-22° is retained in XRD patterns of both BMI-epoxy composites with and without BT nanofiller. From figure 4.7 B, the planes corresponding to BT were clearly visible in the BMI-epoxy-BT composites in addition to the broad XRD pattern of amorphous BMI-epoxy composite.

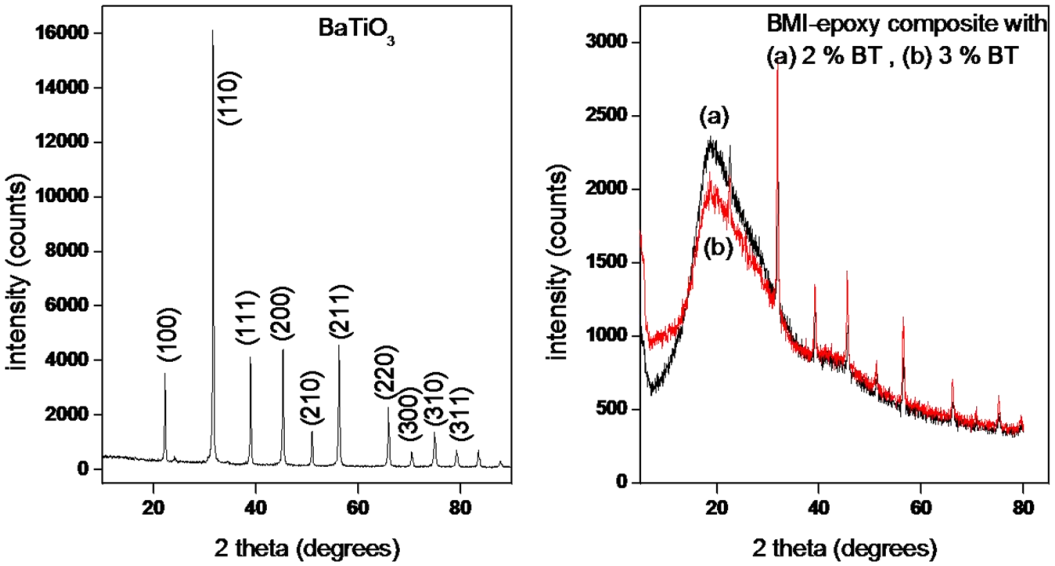

Figure 4.7 X-ray diffraction patterns of (A) synthesised BT nanoparticles (B) BMI-epoxy composite with 2 weight *% BT (a) and BMI-epoxy composite with 3* weight *% BT (b).*

4.3.3.2. X-ray diffraction analysis of BMI resin

The X-ray diffractogram of the unmodified, uncured neat BMI resin (figure 4.8 A) exhibits two halo peaks ranging between 2θ values 10°-35° and 35°-55° respectively. Sharp narrow patterns were also visible over the halo peak observed between 10°-35°. This shows the semi crystalline nature of uncured BMI. XRD pattern of BMI-epoxy composite (figure 4.8 B) shows variation in the diffraction pattern compared to unmodified uncured BMI. The halo peak observed between 2θ values 35°-55° for BMI was almost invisible in the case of BMI-epoxy composite. Sharp narrow peaks observed over the halo peak between 10°-35° were also invisible in BMI-epoxy composite. The changes observed in the XRD patterns of BMI-epoxy composite, in comparison with BMI reveal the structural change that had occurred in the composite due to interaction between BMI and epoxy. The semi crystalline nature of BMI has changed to amorphous when modified with epoxy resin. This could be explained due to the crosslinking bonds formed in the composites facilitated by epoxy resin. In addition to that we could also assume that there is a change in brittle nature of BMI matrix by the addition of epoxy into BMI matrix due to the change from semi crystalline to amorphous nature[45].

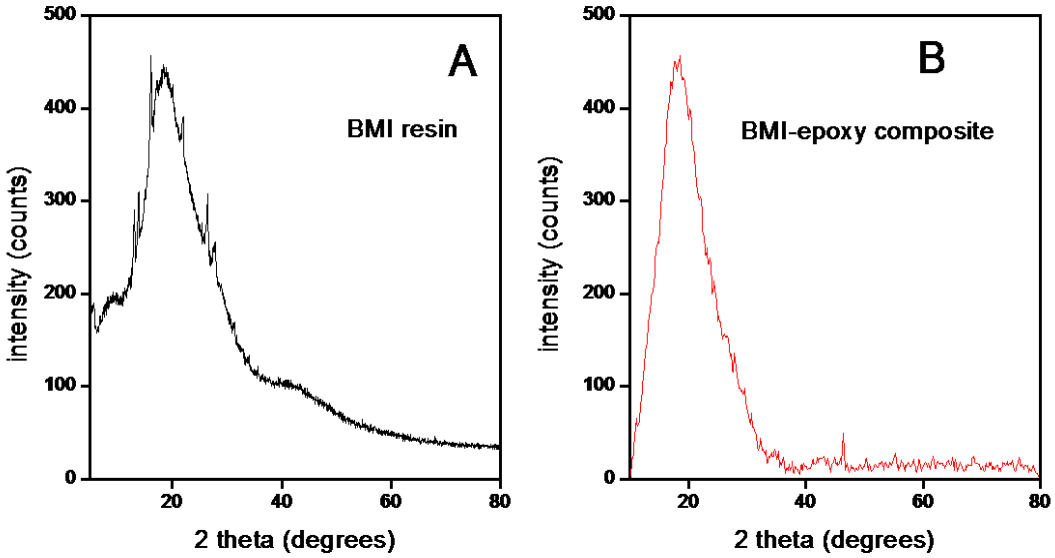

Figure 4.8 X-ray diffraction pattern of (A) unmodified uncured neat BMI resin (B) BMI-epoxy composite.

4.3.4. FTIR analysis

FTIR spectra of $BaTiO_3$ (figure 4.9) exhibited peaks at 630 and 858 cm^{-1} corresponding to the metal-oxygen (Ti-O) stretching vibrations. Peaks at 1641 and 3412 cm^{-1} corresponded to the -OH deformation and stretching vibrations due to the presence of adsorbed -OH group. A weak absorption peak at 1641 cm^{-1} attributed to the bending vibration of H-O-H arose from adsorbed water molecules. A strong peak at 1436 cm^{-1} is related to the C-O stretching vibration that arose from the trace of $BaCO_3$ present in $BaTiO_3$[46].

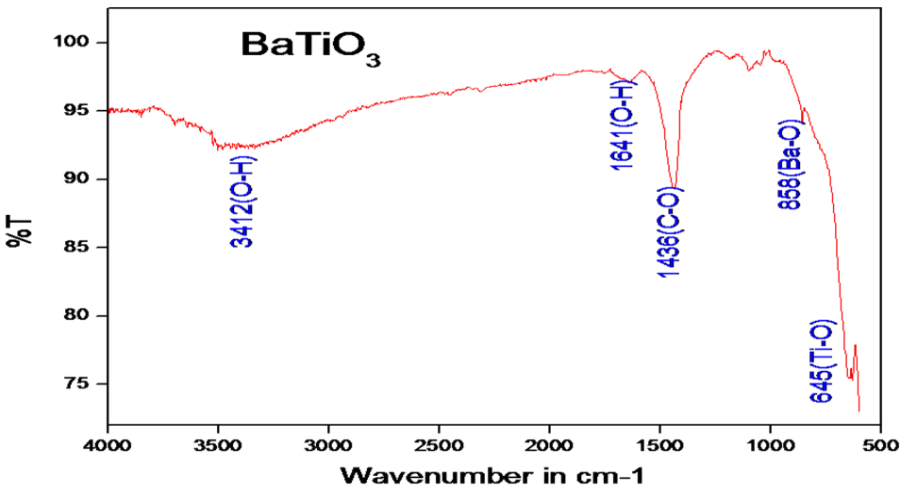

Figure 4.9 FTIR analysis of the synthesised $BaTiO_3$ nanoparticles.

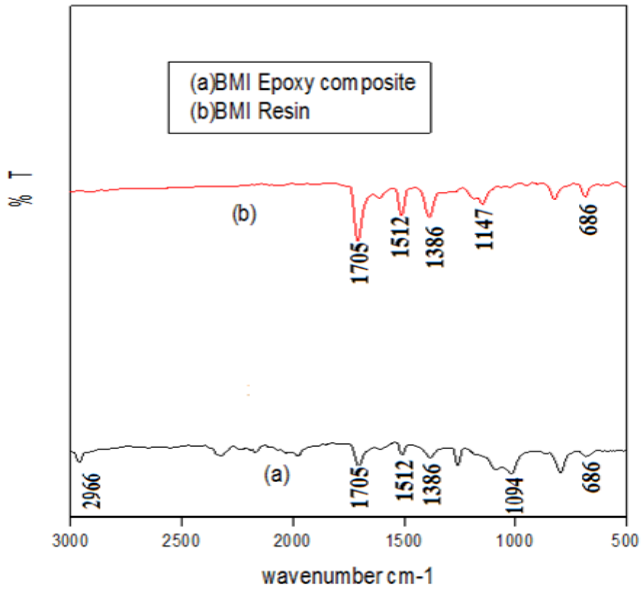

Figure 4.10 FTIR analysis of (a) BMI-epoxy composite (b) unmodified uncured BMI resin.

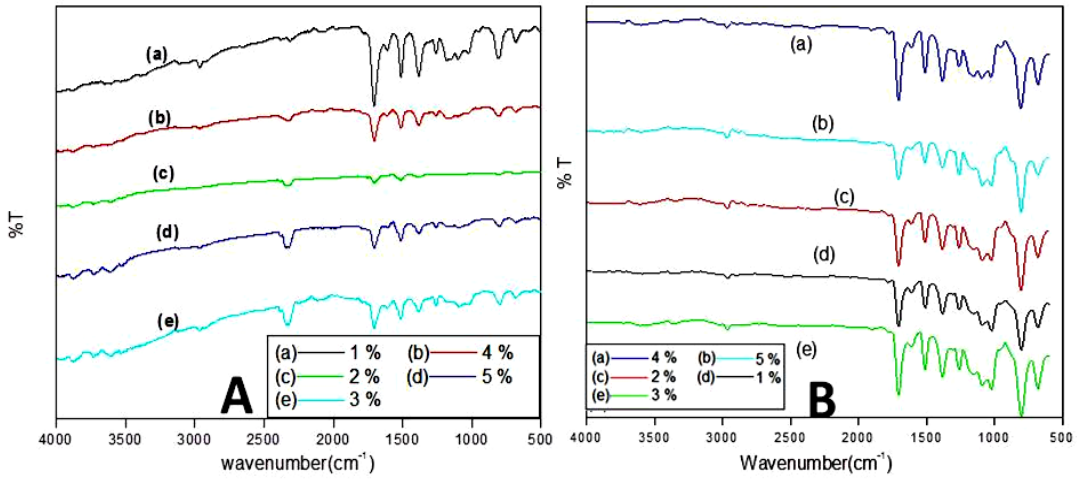

Figure 4.11 FTIR analysis of BMI-epoxy-BT nanocomposites reinforced with (A) EGF (B) SC – EGF.

FTIR spectra of the uncured BMI resin (figure 4.10 b) and the cured BMI-epoxy nanocomposites show a decrease in wavenumber of the strong absorption band at 1147 cm^{-1} due to the maleimide C-N-C stretching vibration to 1094 cm^{-1} during curing, which indicates the conversion of maleimide functionality. In all the cured BMI-epoxy composites and the uncured BMI resin, there is a strong absorption peak at 1705 cm^{-1} indicating the presence of strong C=O asymmetric stretching of the imide group. Peaks at 2341 cm^{-1} and 2320 cm^{-1} arose from the asymmetric stretching mode of CO_2 adsorbed from the atmosphere.

The strong absorption bands due to C-N-C and C-N stretching vibrations were observed at 1147 cm^{-1} and 1386 cm^{-1} respectively. Characteristic absorption bands of maleimide ring were observed at 686 cm^{-1}, 1147 cm^{-1} and 1386 cm^{-1}. C=C stretching was observed at 1510 cm^{-1}. Analysis and comparison of the FTIR absorption spectrum of the cured composites and the uncured BMI resin showed a reduced number of peaks in the range of 600-1600 cm^{-1} indicating the completion of curing process of BMI resin[45,47].

Table.4.3 Tentative assignment of the main absorption bands of FTIR.

IR bands of Uncured BMI (cm^{-1})	**IR bands of BMI-Epoxy nanocomposites (cm^{-1})**					**Tentative assignment**
	1%	**2%**	**3%**	**4%**	**5%**	
3471 (Weak peak)	3495 3392 medium	3396 Very weak	3533	3475 3518 Very weak	3496 3518	Presence Of –OH group
686 1386	680 1382	680 1382	680 1384	682 1384	682 1384	Presence of Maleimide Ring and imide group
1705 (Very strong)	1705 strong	1705 strong	1705 strong	1705 strong	1705 Strong	Presence of C=O group
1512 (strong)	1510 (strong)	1512	1512	1512 (strong)	1512 (strong)	C=C Benzene ring
1147 (strong)	1149 weak	1143 Very weak	Very Weak Hard to find	Very Weak Hard to find	1095	-C-N-C Maleimide group
823 strong	806 strong	808 medium	800 medium	800 strong	798 strong	Benzene ring
950 medium	946 Very weak	941 weak	Very Weak Hard to find	Very Weak Hard to find	Very Weak Hard to find	Benzene ring
3101 medium	3101 Very weak	Very Weak Hard to find	Very Weak Hard to find	3109 weak	2956 weak	-CH- Maleimide
1613 medium	157Very weak	1610 Weak	1623 Weak	1521medium	1595 weak 1510medium	C=C stretching
1024 weak	1020 Weak	1025 weak	Very Weak Hard to find	Very Weak Hard to find	1110 weak	Weak C-N-Stretch

FTIR spectra of EGF and SC-EGF reinforced BMI-epoxy composites with varying weight % (1-5%) are shown in figure 4.11. Comparative studies reveal that the

characteristic peaks are not much altered in differently reinforced BMI-epoxy-BT nanocomposites. The characteristic absorption peak of imide C=O group at 1705 cm^{-1}, the C=C stretching of aromatic rings at 1603-1613 cm^{-1} and the C-C stretching of aromatic ring at 1512 cm^{-1} are retained in both FTIR spectra. In the FTIR spectra of EGF reinforced BMI-epoxy nanocomposites, a small peak between 2873 and 2965 cm^{-1} has been observed due to the C-H stretching of CH_2. More intense peaks are observed in FTIR spectra of SC-EGF reinforced BMI-epoxy nanocomposites.

The IR peak for the oxirane ring of the epoxy resin at 915 cm^{-1} is absent in both the BMI-epoxy composites with and without nanofiller (figure 4.11 & 4.10 a). This suggests the possibility of ring opening and consequent crosslinking between epoxy and BMI. The appearance of very weak OH peak beyond 3500 cm^{-1} due to the opening of the oxirane ring of the epoxy is found in all the BMI-epoxy nanocomposites (figure 4.11) that indicates intercrosslinking between BMI and epoxy resin which proceeds through the ring opening of epoxy (oxirane ring) and formation of -N-CH (OH) CH_2- bonds between N of maleimide ring and –CH of epoxy resin (figure 4.12).

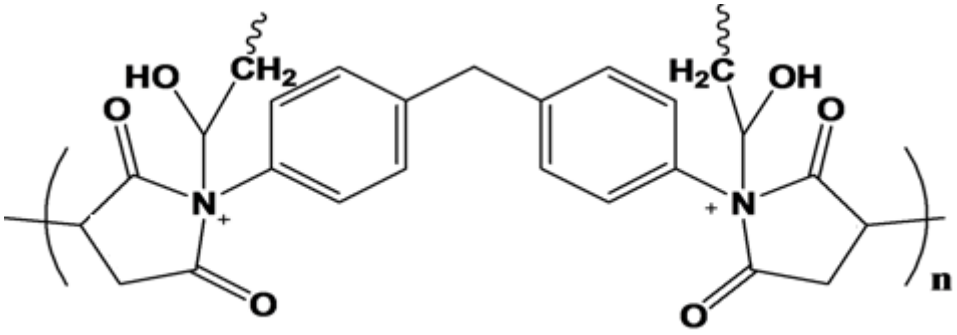

Figure 4.12 Intercrosslinking between BMI and epoxy resin.

4.3.5. Mechanical properties of BMI-epoxy nanocomposites

The flexural and tensile strength of BMI-epoxy-BT nanocomposites measured as per ASTM standards (figure 4.13) is higher than that of BMI-epoxy composite without filler. For samples of BMI-epoxy composites with 1-5 weight % of BT filler, the flexural strength and tensile strength varies with the change in percentage of BT nanoparticles and the maximum value is obtained when the percentage of BT nanoparticles is 2 weight %.

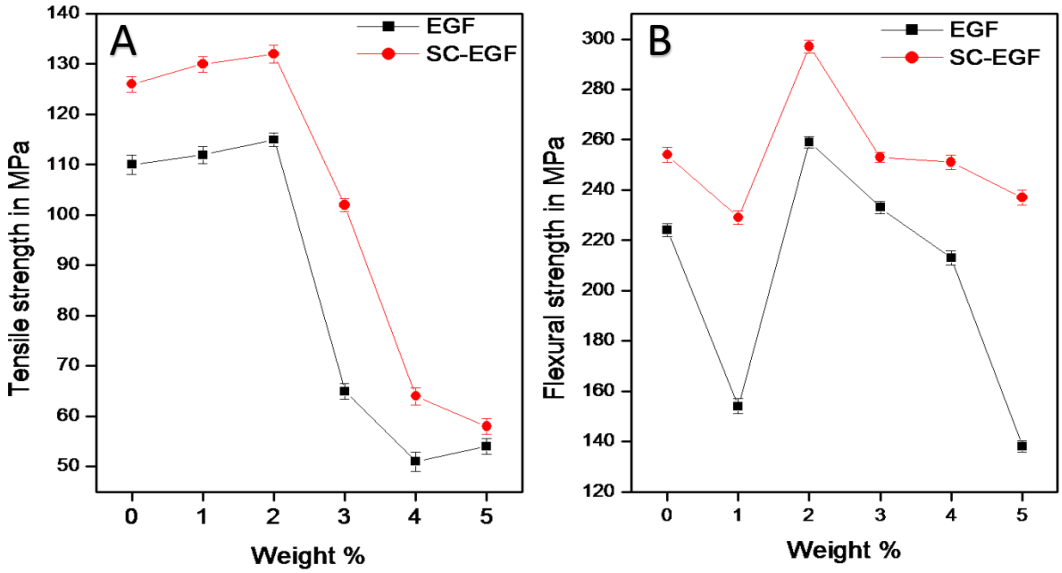

Figure 4.13 Comparative study of effect of weight percentage of BT nanoparticles on tensile strength (A) and flexural strength (B) of BMI-epoxy-BT nanocomposites reinforced with E-glass fiber (EGF) and silane coated E-glass fiber (SC- EGF).

The comparative analysis of the above results showed a remarkable increase in the tensile strength and flexural strength of silane coated E-glass fiber reinforced nanocomposite, establishing the fact that there is a significant interaction between silane coated E-glass fiber and the matrix[48]. The tensile and flexural strength increases first and then decreases with the increase in weight % of nanofiller. The increased rigidity contributed by the loaded nanofiller owing to the increased matrix to filler interaction is responsible for the enhanced tensile and flexural strength. When the weight % of the filler is above a certain value there is a chance for filler agglomeration that may reduce the inter chain interactions resulting in decreased tensile and flexural strength.

4.3.6. Dielectric properties of BMI-epoxy-BT nanocomposites

4.3.6.1. Dielectric permittivity

Figure 4.14 depicts the dependence of dielectric permittivity of BMI epoxy nanocomposites on the weight percentage of BT nanoparticles measured at room temperature in the frequency range 10^1-10^6 Hz. The dielectric permittivity reached a maximum value when the weight % of BT nanoparticles was 2 weight % for both EGF and SC-EGF.

Nanofiller content is responsible for the heterogeneity of the systems and the extended interface. Space charges migrate under the influence of the field and accumulate at the interfaces where they form dipoles with enhanced inertia. This charge trapping procedure at the interface contributes to the dielectric response and permittivity[49]. Dielectric permittivity usually decreases with an increase in frequency ascribed to an interfacial relaxation. Interfacial polarisation has enough time to orient itself in the direction of the alternating field [50].

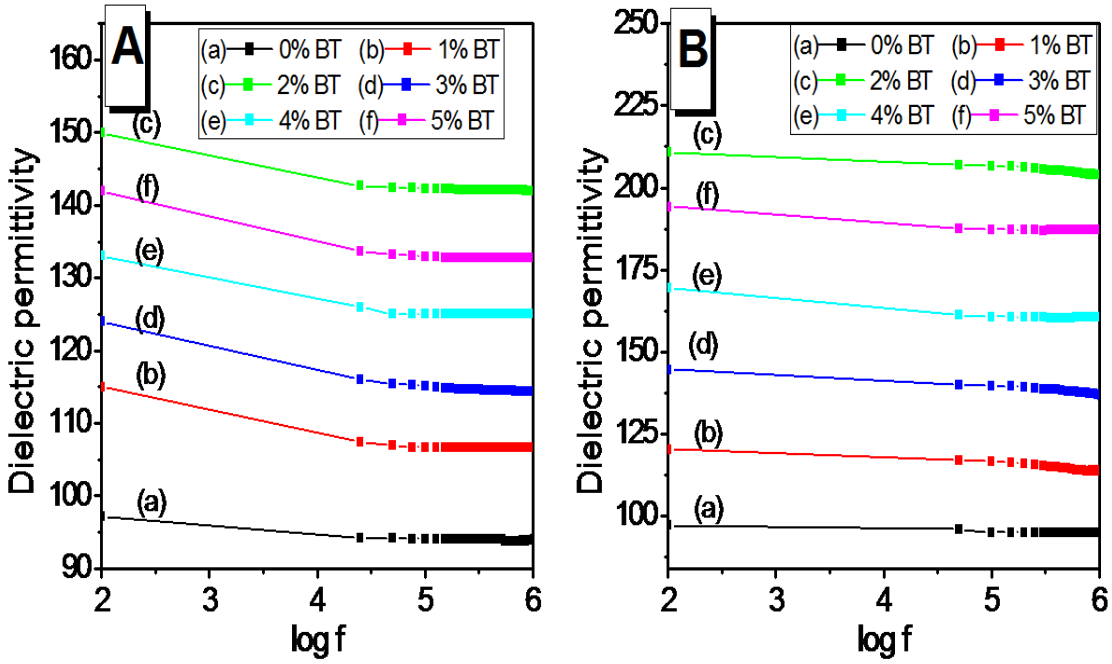

Figure 4.14 Variation of dielectric permittivity with logarithmic frequency of BMI-epoxy-BT nanocomposites reinforced with (A) EGF (B) SC-EGF.

4.3.6.2. Dielectric loss(tan delta)

Electrical conductivity, dielectric polarisation etc., mainly depend on loss tangent or tan δ. Due to the high polarisation of BT nanoparticles compared to that of BMI-epoxy matrix, increased dielectric permittivity was observed. By increasing the percentage of BT nanoparticles, no trends could be seen in the values of the dielectric loss of the composites (figure 4.15). At very small percentage of BT (2 weight %), the dielectric loss of the composite remained very low. BMI-epoxy-BT nanocomposites have attracted much attention in practical applications due to their high dielectric permittivity and low dielectric loss.

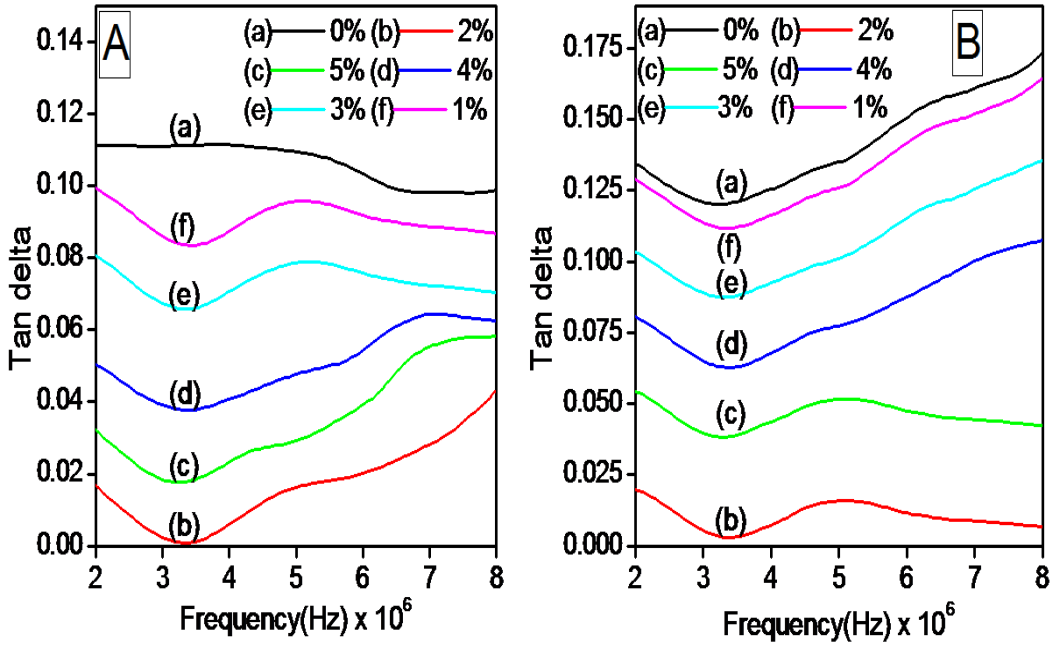

Figure 4.15 Variation of tan delta with frequency of BMI-epoxy-BT nanocomposites reinforced with (A) EGF (B) SC-EGF.

4.3.6.3. Dielectric properties of BMI-epoxy-BT nanocomposites at high frequencies

Dielectric constants and dielectric loss of the fabricated nanocomposites have been obtained at higher frequencies (in GHz) by using a vector network analyser at room temperature and was found to be highest for the BMI-epoxy nanocomposite with 1 weight % BT nanofiller[51] (figure 4.16). Dielectric permittivity depends on the thickness of the sample, uniformity of the surface of the sample, presence of air occupied voids etc. When the weight % of BT nanoparticles is above a certain value, the presence of agglomerated nanofiller at the interface may reduce the formation and accumulation of space charge. This may also lead to a decrease in the rate of charge trapping, so the dipoles get enough time to orient themselves, leading to a decrease in dielectric permittivity. Even in the high frequency range, there may be some charge carriers that cannot absorb energy for breaking the bonds leading to a decrease in dielectric permittivity.

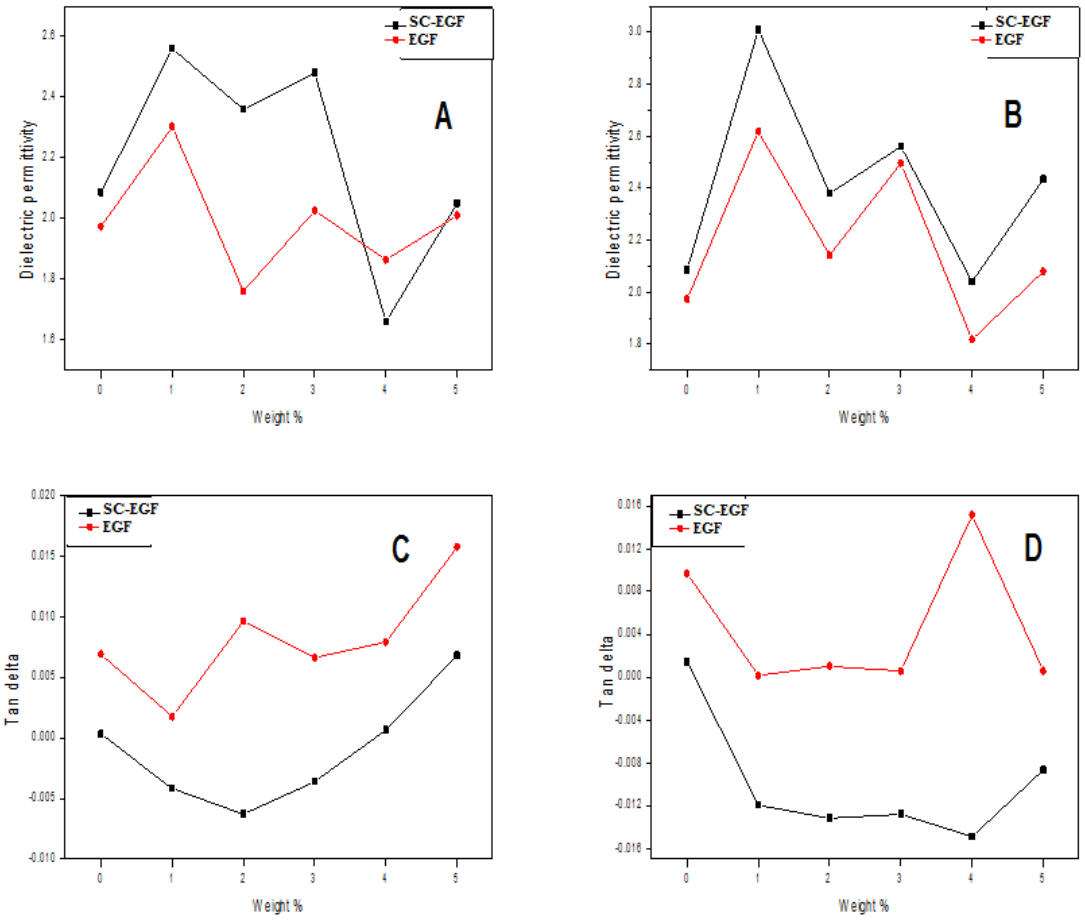

Figure 4.16 Weight percentage–dielectric permittivity graph (A & B) and weight percentage-tan delta graph (C & D) of BMI-epoxy-BT nanocomposites with EGF and SC-EGF at frequencies 3.4240 GHz (A & C) and 5.5868 GHz (B & D).

4.3.6.4 Dielectric strength

The variation of dielectric strength with weight percentage of BT nanoparticle incorporated BMI-epoxy nanocomposites are illustrated in figure 4.17. The energy storage capacity and energy density of polymer nanocomposites depend upon the value of breakdown field strength. The AC breakdown studies were performed on BMI-epoxy nanocomposites as per ASTM D149. Breakdown voltage varies with the material composition, shape of the material and length between the electrical contacts. BMI-epoxy nanocomposite with 3 weight % of BT nanofiller exhibited maximum dielectric strength. Microimperfections caused by the agglomerated BT nanoparticles cause a decrease in dielectric strength whereas the enhancement in the property may be due to the effective dispersion of BT nanoparticles in BMI-epoxy matrix.

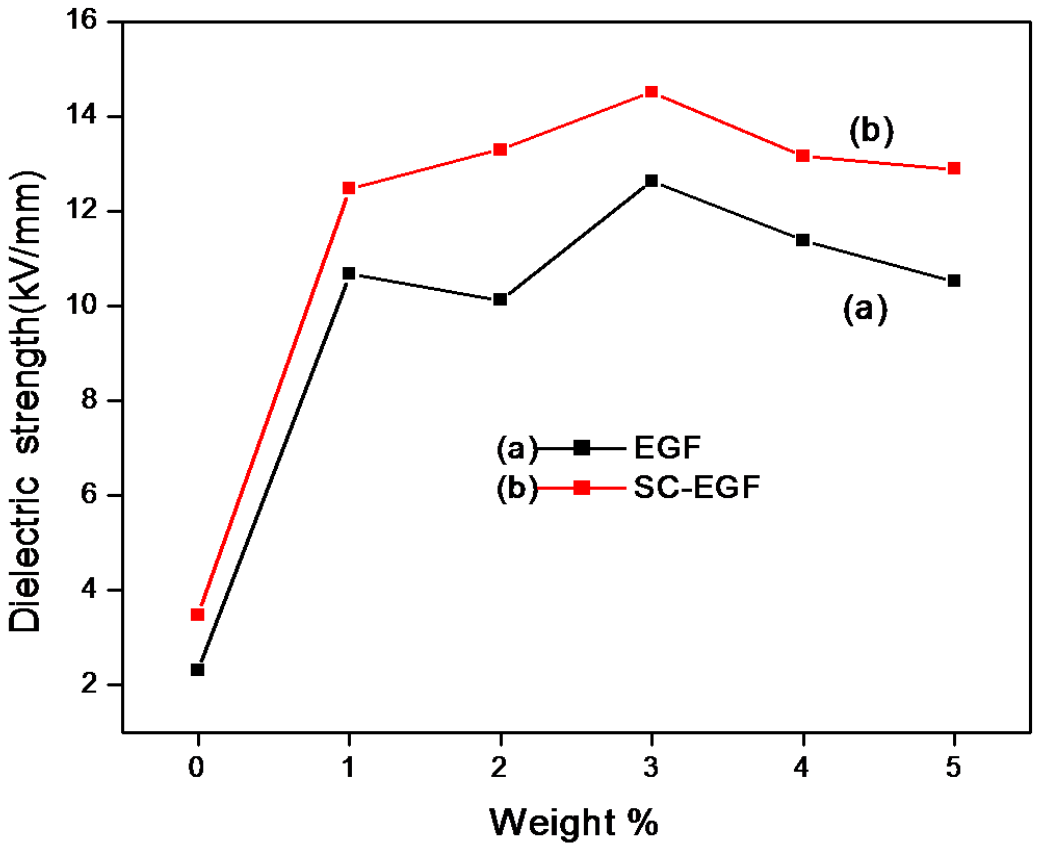

Figure 4.17 Effect of weight percentage of BT nanoparticles of BMI-epoxy composites on dielectric strength.

4.4. Conclusions

Glass fiber reinforced bismaleimide-epoxy composite and bismaleimide-epoxy nanocomposite with $BaTiO_3$ nanoparticles at different filler loadings have been prepared. The effect of $BaTiO_3$ nanoparticles on the mechanical, thermal and dielectric properties of bismaleimide-epoxy composites was studied. Both glass fiber reinforced (EGF & SC-EGF) BMI-epoxy-$BaTiO_3$ nanocomposites with 3 weight % of $BaTiO_3$ have better insulating properties and with 2 weight % exhibits better mechanical properties. Dielectric constants and dielectric loss of the fabricated nanocomposites have been obtained at higher frequencies (in GHz) by using a vector network analyser at room temperature and was found to be highest for the BMI-epoxy nanocomposite with 1 weight % nanofiller. Tensile strength of BMI-epoxy nanocomposites with 2 weight % BT nanofiller was increased 1.05 times in EGF and 1.10 times in SC-EGF reinforced composites as compared to the composite without filler whereas the flexural strength of the above composites was increased 1.16 and 1.17 times respectively with

EGF and SC-EGF reinforcement as compared to the composite without filler. The enhancement in dielectric strength of BMI-epoxy nanocomposite with 2 weight % BT nanofiller was found to be 2.68 and 3.80 times respectively with EGF and SC-EGF reinforcement compared to the composite without filler. This significant enhancement in tensile and flexural strength as well as in dielectric strength may be due to greater interaction between SC-EGF and the BMI-epoxy matrix. Maximum dielectric constant and minimum dielectric loss was exhibited by BMI-epoxy nanocomposite with 2 weight % of BT nanofiller.

References

1. Hu, J., Gu, A., Liang, G., Zhuo, D. & Yuan, L. Preparation and properties of mesoporous silica/bismaleimide/diallyl bisphenol composites with improved thermal stability, mechanical and dielectric properties. Express Polym. Lett. 5, 555–568 (2011).
2. Xu, W. et al. High permittivity nanocomposites fabricated from electrospun polyimide/$BaTiO_3$ hybrid nanofibers. Polym. Compos. 37, 794–801 (2016).
3. Jin, L., Agag, T. & Ishida, H. Bis(benzoxazine-maleimide)s as a novel class of high performance resin: Synthesis and properties. Eur. Polym. J. 46, 354–363 (2010).
4. Lu, G. & Huang, Y. Preparation and characterisation of Bismaleimide resin/titania nanocomposites via sol-gel process. arXiv Prepr. arXiv1304.7082 (2013).
5. Rajabi, L. & Malekzadeh, G. Effects of bismaleimide resin on dielectric and dynamic mechanical properties of epoxy-based laminates. Iran. Polym. J. (English Ed. 15, 447–455 (2006).
6. Mahesh, K. P. O., Alagar, M. & Kumar, R. S. Synthesis and characterisation of polyurethane-toughened epoxy-bismaleimide matrices. High Perform. Polym. 16, 391–404 (2004).
7. Chandra, R. & Rajabi, L. Recent Advances in Bismaleimides and Epoxy-Lmide/ Bismaleimide Formulations and Composites. J. Macromol. Sci. Part C 37, 61–96 (1997).
8. Seo, J., Jang, W. & Ham, H. Thermal properties and water sorption behaviors of epoxy and bismaleimide composites.pdf. Macromol. Res. 15, 10–16 (2007).
9. Rozenberg, B. A., Dzhavadyan, E. A., Morgan, R. & Shin, E. High-performance bismaleimide matrices: Cure kinetics and mechanism. Polym. Adv. Technol. 13, 837–844 (2002).
10. Stenzenberger, H. Recent advances in thermosetting polyimides. Br. Polym. J. 20, 383–396 (1988).
11. Nalwa, H. S. Handbook of low and high dielectric constant materials and their applications, two-volume set. (Elsevier, 1999).
12. Barber, P. et al. Polymer Composite and Nanocomposite Dielectric Materials for Pulse Power Energy Storage. Materials (Basel). 2, 1697–1733 (2009).
13. Gu, A. High performance bismaleimide/cyanate ester hybrid polymer networks with excellent dielectric properties. Compos. Sci. Technol. 66, 1749–1755 (2006).
14. Jaffe, H. Piezoelectric ceramics. J. Am. Ceram. Soc. 41, 494–498 (1958).
15. Cross, L. E. Dielectric, piezoelectric, and ferroelectric components. Am. Ceram. Soc. Bull. 63, 586–590 (1984).
16. Moulson, A. J. & Herbert, J. M. Electroceramics: materials, properties, applications. (John Wiley & Sons, 2003).
17. Phule, P. P. & Risbud, S. H. Low-temperature synthesis and processing of electronic materials in the BaO-TiO_2 system. J. Mater. Sci. 25, 1169–1183 (1990).
18. Hilton, A. D. & Frost, R. Recent developments in the manufacture of barium titanate powders. in Key Engineering Materials vol. 66 145–184 (1992).

19. Newnham, R. E. Electroceramics. Reports Prog. Phys. 52, 123 (1989).
20. Padmini, P., Hari, N. S. & Kutty, T. R. N. Cryogenic sensors from semiconducting barium titanate ceramics with strong negative temperature coefficient of resistance. Sensors Actuators A Phys. 50, 39–44 (1995).
21. Smith, D. S. et al. Transient thermal gradients in barium titanate positive temperature coefficient (PTC) thermistors. J. Am. Ceram. Soc. 81, 1789–1796 (1998).
22. Capurso, J. S., Alles, A. B. & Schulze, W. A. Processing of laminated barium titanate structures for stress-sensing applications. J. Am. Ceram. Soc. 78, 2476–2480 (1995).
23. Tomonori, Ik. K., Okudaira; Hiromi Itoh, all of H. & Japan. United States Patent. (1996).
24. Wang, X. et al. Glass additive in barium titanate ceramics and its influence on electrical breakdown strength in relation with energy storage properties. J. Eur. Ceram. Soc. 32, 559–567 (2012).
25. Niu, Y. et al. Effect of the modifier structure on the performance of barium titanate/poly (vinylidene fluoride) nanocomposites for energy storage applications. ACS Appl. Mater. Interfaces 7, 24168–24176 (2015).
26. Li, W.-B., Zhou, D., Pang, L.-X., Xu, R. & Guo, H.-H. Novel barium titanate based capacitors with high energy density and fast discharge performance. J. Mater. Chem. A 5, 19607–19612 (2017).
27. Chu, L. W., Prakash, K. N., Tsai, M.-T. & Lin, I.-N. Dispersion of nano-sized $BaTiO_3$ powders in nonaqueous suspension with phosphate ester and their applications for MLCC. J. Eur. Ceram. Soc. 28, 1205–1212 (2008).
28. He, Y. et al. Sensors and Actuators B : Chemical Humidity sensing properties of $BaTiO_3$ nanofiber prepared via electrospinning. Sensors Actuators B. Chem. 146, 98–102 (2010).
29. Singh, M., Yadav, B. C., Ranjan, A., Kaur, M. & Gupta, S. K. Sensors and Actuators B : Chemical Synthesis and characterisation of perovskite barium titanate thin film and its application as LPG sensor. Sensors Actuators B. Chem. 241, 1170–1178 (2017).
30. Wegmann, M., Brönnimann, R., Clemens, F. & Graule, T. Barium titanate-based PTCR thermistor fibers: Processing and properties. Sensors Actuators A Phys. 135, 394–404 (2007).
31. Alles, A. B. & Burdick, V. L. Grain boundary oxidation in PTCR barium titanate thermistors. J. Am. Ceram. Soc. 76, 401–408 (1993).
32. Abel, S. et al. A strong electro-optically active lead-free ferroelectric integrated on silicon. Nat. Commun. 4, 1–6 (2013).
33. Singh, U. B., Dhar, R., Dabrowski, R. & Pandey, M. B. Enhanced electro-optical properties of a nematic liquid crystals in presence of $BaTiO_3$ nanoparticles. Liq. Cryst. 41, 953–959 (2014).
34. Barber, P. et al. Polymer composite and nanocomposite dielectric materials for pulse power energy storage. Materials vol. 2 (2009).
35. Chandra, R. & Rajabi, L. Recent Advances in Bismaleimides and Epoxy-Lmide/ Bismaleimide Formulations and Composites. J. Macromol. Sci. Part C Polym. Rev. 37, 61–96 (1997).
36. Mao, Y., Zhou, H. & Wong, S. S. Synthesis, Properties, and Applications of Perovskite-phase Metal Oxide Nanostructures. Mater. Matters 5, 50–53 (2010).
37. Kareiva, A., Tautkus, S., Rapalaviciute, R., Jørgensen, J. E. & Lundtoft, B. Sol-gel synthesis and characterisation of barium titanate powders. J. Mater. Sci. 34, 4853–4857 (1999).
38. Clark, I. J., Takeuchi, T., Ohtori, N. & Sinclair, D. C. Hydrothermal synthesis and characterisation of $BaTiO_3$ fine powders: precursors, polymorphism and properties. J. Mater. Chem. 9, 83–91 (1999).
39. Gromada, M., Biglar, M., Trzepieciński, T. & Stachowicz, F. Characterization of $BaTiO_3$ piezoelectric perovskite material for multilayer actuators. Bull. Mater. Sci. 40, 759–771 (2017).
40. Park, J. H. et al. Synthesis, structure and dielectric properties of $BaTiO_3$ nanoparticles.

J. Korean Phys. Soc. 49, 680–683 (2006).
41. Al-Shakarchi, E. K. & Mahmood, N. B. Three Techniques Used to Produce $BaTiO_3$ Fine Powder. J. Mod. Phys. 02, 1420–1428 (2011).
42. Zheng, C., Cui, B., You, Q. & Chang, Z. Characterization of $BaTiO_3$ Powders and Ceramics Prepared Using the Sol-gel Process, with Triton X-100 Used as a Surfactant. Sci. Res. 341–346 (2010).
43. Zheng, H., Zhu, K., Wu, Q., Liu, J. & Qiu, J. Preparation and characterisation of monodispersed $BaTiO_3$ nanocrystals by sol-hydrothermal method. J. Cryst. Growth 363, 300–307 (2013).
44. Corcione, C. E. & Frigione, M. Characterization of Nanocomposites by Thermal Analysis. Materials (Basel). 5, 2960–2980 (2012).
45. Chandran M, S., Krishna, M., Salini, K. & Rai, K. S. Preparation and characterisation of chain-extended bismaleimide/carbon fibre composites. Int. J. Polym. Sci. 2010, (2010).
46. Mai, T. T. et al. Enhancement of polarisation property of silane-modified $BaTiO_3$ nanoparticles and its effect in increasing dielectric property of epoxy/$BaTiO_3$ nanocomposites. J. Sci. Adv. Mater. Devices 1, 90–97 (2016).
47. Rozenberg, B. A., Dzhavadyan, E. A., Morgan, R. & Shin, E. High-performance bismaleimide matrices: cure kinetics and mechanism. Polym. Adv. Technol. 13, 837–844 (2002).
48. Kanag, S. Y., Anandan, Y. K., Vaidyanath, P. & Baskar, P. Strength properties of coated E-glass fibres in concrete. Gradjevinar 68, 697–703 (2016).
49. Manika, G. C. & Psarras, G. C. Barium titanate/epoxy resin composite nanodielectrics as compact capacitive energy storing systems. Express Polym. Lett. 13, (2019).
50. Wan, L., Zhang, X., Wu, G. & Feng, A. Thermal conductivity and dielectric properties of bismaleimide/cyanate ester copolymer, High Volt. 2, 167–171 (2017).
51. Chakyar, S. P., K. Simon, S., Bindu, C., Andrews, J. & Joseph, V. P. Complex permittivity measurement using metamaterial split ring resonators. J. Appl. Phys. 121, (2017).